

Infrared emitting PbSe nanocrystals for telecommunications window applications

C. E. FINLAYSON[†], A. AMEZCUA[†], P. J. A. SAZIO^{*†}, P. S. WALKER[‡],
M. C. GROSSEL[‡], R. J. CURRY[§], D. C. SMITH[¶] and J. J. BAUMBERG[¶]

[†]Optoelectronics Research Centre (ORC), University of Southampton,
Southampton SO17 1BJ, UK

[‡]School of Chemistry, University of Southampton, Southampton SO17 1BJ, UK

[§]Advanced Technology Institute, School of Electronics and Physical Sciences,
University of Surrey, Guildford, Surrey GU2 7XH, UK

[¶]School of Physics and Astronomy, University of Southampton, Southampton
SO17 1BJ, UK

(Received 7 October 2004)

We demonstrate the colloidal synthesis of PbSe nanocrystal quantum dots, via an organometallic-precursor route, developed from recently reported techniques. This synthesis typically yields a particle size distribution of approximately 5–10%, as may be inferred from the sharp spectral features seen in absorption and from our effective-mass model correlating spectral features to nanocrystal size. An accurate quantitative analysis, using an infrared reference dye, shows these nanocrystals to exhibit infrared photoluminescence from intrinsic quantum-confined states, with high quantum efficiencies of up to 60% in solution. The wavelength of the photoluminescence may also be conveniently size tuned in order to access the 1.3–1.5 μm ‘telecommunications window’. We discuss the significance of this work in the context of future optoelectronic applications.

1. Introduction

Semiconductor nanocrystals represent almost ideal ‘particle-in-a-box’ quantum-mechanical systems for the creation of artificial atoms. In particular, nanometre-sized, roughly spherical colloidal particles of II–VI and III–V materials have aroused great interest owing to the regime of extreme quantum confinement possible when the particle dimensions are smaller than that of the bulk-exciton Bohr radius [1–3]. When this criterion is satisfied, one can think of the nanocrystals as being quasi zero-dimensional systems (‘quantum dots’) with discrete electron and hole states [4], thus greatly altering the usual intraband scattering and relaxation processes seen in bulk semiconductors [5]. Commensurately, such quantum dots also exhibit strongly size-tuneable optical transitions [6]. Common material systems, in which quantum dots have been successfully characterised, include CdSe and CdS [7], operating in the visible region of the spectrum, and InAs [8] in the near infrared. These unique

*Corresponding author. Email: pjas@soton.ac.uk

properties have attracted a diverse range of potential applications, most notably in light-emitting diodes [9], photovoltaic and solar cells [10, 11], lasers and optical gain media [12, 13], photonics [14, 15], biological fluorescence labelling [16] and as components in molecular electronics [17].

One particular area of current interest is in the synthesis and characterization of quantum dots with luminescence which may be size tuned to coincide with the technologically important 1.3–1.55 μm region of the spectrum: the so-called ‘telecommunications window’. Recently, Klimov and co-workers [18] have suggested that optical gain phenomena, such as amplified spontaneous emission, are achievable in thin films of infrared-emitting PbSe nanocrystals. This suggests that such materials have great potential as a possible alternative to the rare-earth dopants currently used in fibre amplifiers [19], which suffer the well-documented drawback of quenching at high concentration and require fairly wavelength-specific optical pumping mechanisms.

Following on from the pioneering work done concerning the organometallic synthesis of visible-light-emitting semiconductor nanocrystals by pyrolysis [20, 21], several different synthesis strategies have been reported for narrow band-gap II–VI infrared emitters. The most notable of these is the work of Wehrenberg *et al.* [22] and Du *et al.* [23], and also a solvothermal route devised by Gautam and Seshadri [24]. All these syntheses also benefit from relatively low reagent toxicity and air sensitivity. In this paper we report the synthesis of stable robust PbSe colloidal nanocrystals, via an organometallic route, using methods derived from some recently reported modifications to conventional routes [25, 26]. Our experiments have helped to address important issues arising out of these routes regarding the optimal conditions needed for control of particle growth. We also address the critical subject of photoluminescence (PL) efficiency (quantum yield) in our samples in a fully quantitative and accurate fashion.

2. Synthesis

The conventional methodology underlying the preparation of size-controlled PbSe quantum dots requires the synthesis of stable precursors of lead and selenium, which are then combined at room temperature under an inert atmosphere. This stock solution is then rapidly injected into a comparable volume of a coordinating solvent at a high temperature, which has the effect of stripping away the protective organic components of the precursors, allowing them to react, giving rise to Pb(II)Se which forms a black insoluble solid and precipitates out of solution. We have explored, however, a more convenient ‘one-pot’ method of thermosolvolytic precipitation, which offers greater control over important parameters, such as reaction temperature and component concentration.

High-quality starting materials for this process were identified as ACS grade Pb(II) acetate and high-purity elemental selenium. The required organometallic lead component, Pb(II) oleate, was prepared by suspending Pb(II) acetate.3H₂O (0.76 g, 2 mmol) and oleic acid (2.82 g, 10 mmol) in a 100 ml round-bottomed flask containing 40 mL of diphenyl ether. This suspension was placed on a rotary pump evaporator for 1 h at a temperature of 95°C. This process replaces acetic acid with oleic acid, thus stabilizing the Pb(II) cation. The process additionally distills off the displaced acetic acid and any residual water of crystallization from the original salt.

The selenium precursor, trioctylphosphine selenide (TOPSe), was prepared by dissolving selenium pellets directly into trioctylphosphine (TOP) to provide a 1 M solution. Rapid stirring over the course of several hours was required to dissolve the pellets and care was taken to maintain an inert environment.

A typical experimental run involved placing freshly prepared Pb(II) oleate solution (2 mmol of lead) with a large stirrer bar into a three-necked flask under a constant flow of nitrogen. This flask was then placed into a temperature-feedback controlled heating mantle at the required reaction temperature and allowed to equilibrate. 6 mL of TOPSe (6 mmol selenium) was then rapidly injected into the hot flask whilst maintaining inert conditions by injection through a septum. Aliquots (about 1 ml) of the proceeding reaction were taken at noted time intervals to permit the later examination of the time course of nanoparticle growth. Aliquots were directly injected into an excess volume of methanol at room temperature to inhibit further reaction and to dissolve out the undesired solvent, unbound coordinating molecules and unreacted precursors.

The synthesis is essentially a three-step process of nucleation, growth and ripening. Suitable experimental conditions and control of component stoichiometry allow for each of these steps, to some extent, to be controlled independently. The nucleation phase is primarily influenced by the temperature of the reaction vessel. Higher temperatures cause rapid and complete nucleation of the available precursors, with little or no growth from solution commensurately, whereas lower temperatures result in low reaction rates due to increased precursor stability. In practice, reaction temperatures in the range of 70–120°C were used. We also find that the growth phase is critically dependent on the lead:selenium ratio. Clearly, the lead and selenium precursors always react with ratio 1:1; however, the different binding strengths of the oleic acid and TOP ligands have important consequences for the availability of free lead and selenium atoms during the dynamic phase of crystalline growth.

We have experimented with these factors by varying the concentrations of TOP (soft Lewis base) and oleic acid (hard base) in standardized reactions and also observe that this affects not only the growth rate but also the size distributions of the resultant nanoparticle ensembles. Most interestingly, it was found that any uncoordinated TOP from the TOPSe precursor plays a pivotal role in the growth stage and this may be due to the premature stabilization of the surfaces of nascent nanocrystals, rather than an issue surrounding precursor stability. We speculate that high concentrations of TOP within the reaction vessel may cause a high fraction of the nanocrystal surface sites to become TOP coordinated rather than solvent coordinated, leading to a retardation of the growth rate and a departure from the desired 'size-focusing' regime. This problem may indeed be exacerbated by the disproportionate quantities of TOPSe used in many reported methods.

On a related issue, it was also found that the reaction is sensitive to the purity of the TOP used. We find that the rapid rates of reaction seen if freshly distilled high-purity TOP is used are not, in fact, conducive to the effective control of particle growth. However, in common with other alkyl phosphines, TOP will gradually oxidize to trioctylphosphine oxide (TOPO) if exposed to air and a large concentration of TOPO can potentially build up before any physical signs, such as the formation of solid crystals of TOPO, are noticeable. An ideal TOPO impurity concentration, where reaction rates and control over growth are optimal, is often seen some days or weeks after distillation of the TOP and the commercially available

'tech-grade' TOP often produces satisfactory results. This synthesis does not appear to yield any useful product if the TOPO impurity content is subsequently allowed to increase still further over time.

The effects of the ripening phase should be an increase in nanocrystal size, with a corresponding red shift in the relevant spectral peaks, as smaller particles coalesce (Ostwald ripening [27]). However, the ripening stage is difficult to isolate and in this context is effectively subsumed into the growth phase. When the required nanocrystal size is reached, the reaction may be terminated by removal of the heat and the addition of a large excess of methanol into the vessel. The reaction product samples were treated to mild centrifugation (about $5000 \text{ rev min}^{-1}$), which facilitated precipitation of the brown–black product. The methanol solution was decanted away and the product dried under a stream of nitrogen. The resultant oleic acid capped PbSe nanocrystals were stored under nitrogen and wrapped in aluminium foil until required. Subsequent spectroscopic analysis was carried out using samples dispersed into hexanes. The longevity of PbSe stored dissolved in hexane, or any other solvent, was not explored; however, we note that commercially available material is routinely stored and delivered in hexane.

3. Characterization

Absorption spectra of aliquots taken from a particular synthesis are shown in figure 1. The injection and growth temperature were 100°C and the aliquots were redispersed in hexanes and analysed using a dual-beam ultraviolet–visible–nearinfrared absorption spectrometer, using a hexanes-only reference cell. The spectra clearly

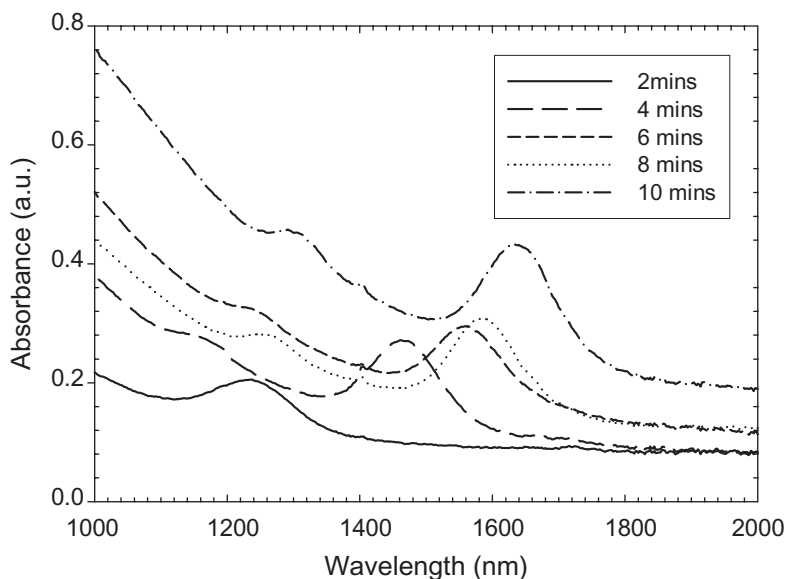


Figure 1. Absorption spectra taken from aliquots of a representative synthesis of PbSe nanocrystals, showing the size tuning of the transition peak features with increased growth time in 2 min steps from 2 to 10 min after injection (a.u., arbitrary units). The broadening of these features is predominantly related to the inhomogeneous size distribution.

demonstrate the time course of the reaction, with the principal transition (1S(h)–1S(e)) absorption peak of the PbSe nanocrystals being size tuned from $\lambda = 1200$ nm to 1600 nm between 2 and 10 min after injection. The second exciton peak (1P(h)–1S(e)) can also be seen at higher energies in some of the later spectra. These results demonstrate how the principal absorption peak may be effectively tuned across the 1.3–1.55 μm telecommunications window wavelengths. The much larger Bohr exciton radius of PbSe (about 46 nm) relative to wide-band-gap II–VI semiconductors, such as CdSe, means that a very wide range of absorption wavelengths, from the visible up to around 4 μm , may be sampled by tuning the particle size in the 1–40 nm regime.

We have developed an effective-mass model of the 1S(e) and 1S(h) bands, for a spherical PbSe nanoparticle, in order to derive the particle dimensions from the absorption peaks of our data [28, 29]. By using appropriate values for the conduction-electron and valence-hole effective masses and taking the bulk band-gap energy of PbSe to be 0.28 eV, we are able to employ a ‘particle confined in a sphere’ type of approach to calculate the shift in energy of the 1S levels as a function of particle size, relative to the bulk values. We assume that the spacing of the 1S(e) and 1S(h) levels subsequently defines the band-gap energy. Figure 2 shows how the predicted band-gap energy and hence the peak absorption wavelength are expected to vary with changing particle diameter. From this, we can say that diameters in the approximate range 7.7–8.5 nm are needed to access telecommunication-window wavelengths and, indeed, the absorption spectra in figure 1 suggest that the mean particle diameter was tuned from around 7.3 nm through to 9.4 nm in that particular synthesis. By comparison of the observed broadening of the absorption peaks to the corresponding interpolated nanocrystal-size points in our model, we can also infer the inhomogeneous size distribution. For example, in figure 1, we have an exciton linewidth $\Delta\lambda$ of 146 nm for the 4 min peak at around $\lambda = 1460$ nm, assuming

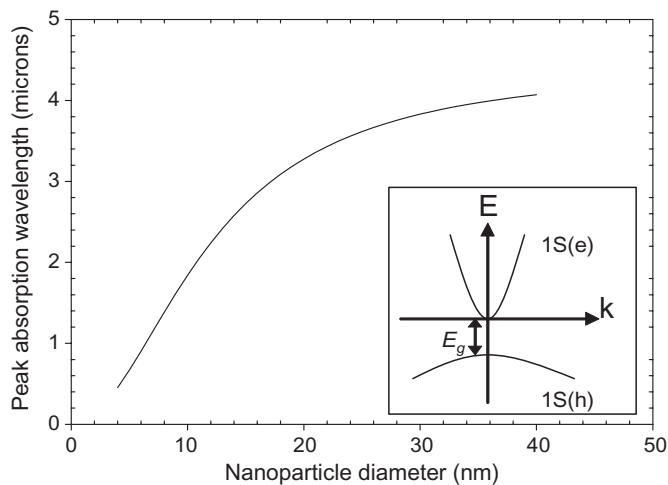


Figure 2. A two-level effective-mass model, predicting the variation in absorption peak wavelength with nanocrystal diameter, for spherical PbSe nanoparticles. The parameters used in this model were $E_g = 0.28$ eV, $m^*(e) = 0.084m$ and $m^*(h) = 0.70m$, where E_g is the bulk band-gap energy and m is the electron rest mass. The inset shows a schematic band diagram for the 1S(e) and 1S(h) states of the PbSe system.

a simple Gaussian line shape. In this case, the mean diameter d is calculated to be 8.32 nm, with the full width at half-maximum giving a Δd of 0.54 nm, implying a $\Delta d/d$ size distribution of 6.5%.

In order to investigate any photoluminescent properties that the synthesized PbSe quantum dots may possess, solutions of the samples in hexanes were placed into fluorimetry-grade silica cuvettes and excited with a $\lambda = 808$ nm diode laser. The resultant luminescence was analysed using a standard collimation and monochromator arrangement and an InGaAs detector, with lock-in amplification. In figure 3, typical PL spectra are shown together with a corresponding absorption spectrum. In common with previous reports in the literature, we observe the PL to exhibit the same inhomogeneous broadening effects as seen in absorption and to be somewhat Stokes shifted, owing to a fine-structure splitting of hole states, not accounted for in the simple effective-mass model described above [30]. Commensurate to our ability to size-tune the absorption features of the PbSe nanocrystals across the telecommunication window, we are also able to size-tune the PL in a similar fashion. The PL emission in solution is also observed to be stable, even under continuous excitation in air at room temperature.

Of particular importance to the use of these materials in future applications is the issue of achieving high quantum yields (or PL efficiency) and the ability to measure and calculate this accurately. Although some rather cursory values have been previously quoted regarding PbSe nanocrystals [22, 23], we note that the correct method of calculating PL efficiencies of semiconductor materials has historically been an issue of some controversy [31]. Here, we describe a technique of quantitative comparison between the sample PL and that from an infrared dye of known quantum yield, ‘indocyanine green’ in dimethylsulphoxide (DMSO).

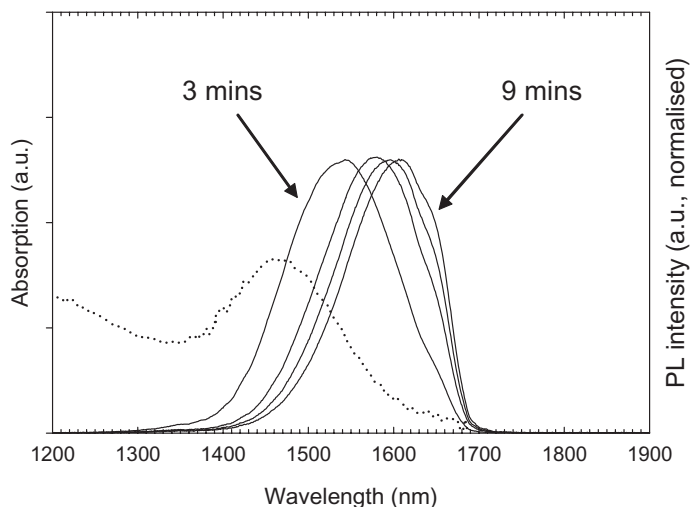


Figure 3. Sequential normalized PL spectra of aliquots of PbSe nanocrystals taken from a reaction at 3, 5, 7 and 9 min after injection, which have been redispersed in hexanes and placed in a fluorimetry cuvette (a.u., arbitrary units). Our effective-mass model suggests corresponding mean particle diameters of 8.07, 8.40, 8.45 and 8.48 nm, respectively. This clearly shows how the PL may be size tuned across the near-infrared spectrum, including the 1.3–1.55 μm telecommunications window. The absorption spectrum of the 3 min aliquot is also shown for reference.

A rigorous ‘photon-out–photons-in’ method of calculating the solution PL efficiencies of our samples was used.

Firstly, the optical densities of the sample and reference solutions were matched as closely as possible at the wavelength of the diode laser excitation source (808 nm), with both solutions placed into fluorimetry cuvettes of identical geometries and path lengths. Care was taken not to exceed an optical density of 0.1 in either cuvette, as this might lead to problems of self-absorption. Next the PL from the cuvettes was detected using the same detection set-up as described above. The geometries and circumstances of excitation and detection were therefore *identical* for sample and reference. Finally, the resultant PL spectra were compared in order to calculate an accurate PL efficiency for the PbSe nanocrystal sample. Figure 4 shows such a comparison, with the absorption spectrum of the reference dye also shown for completeness.

Clearly, if we take the standard definition of quantum yield as being

$$QY = \frac{\text{number of photons emitted}}{\text{number of photons absorbed}}$$

then a method of merely comparing the areas under the two PL spectra in figure 4 is not adequate, as the photon energy is a function of wavelength and a higher photon flux is required at longer wavelengths to produce the same irradiance per unit area than at shorter wavelengths. In addition, the sensitivity response of the detector as a function of wavelength must be corrected for. The formula used in all our subsequent calculations was therefore

$$QY = \frac{\varepsilon \int \lambda I_{\text{sample}}(\lambda) R(\lambda) d\lambda}{\int \lambda I_{\text{ref}}(\lambda) R(\lambda) d\lambda},$$

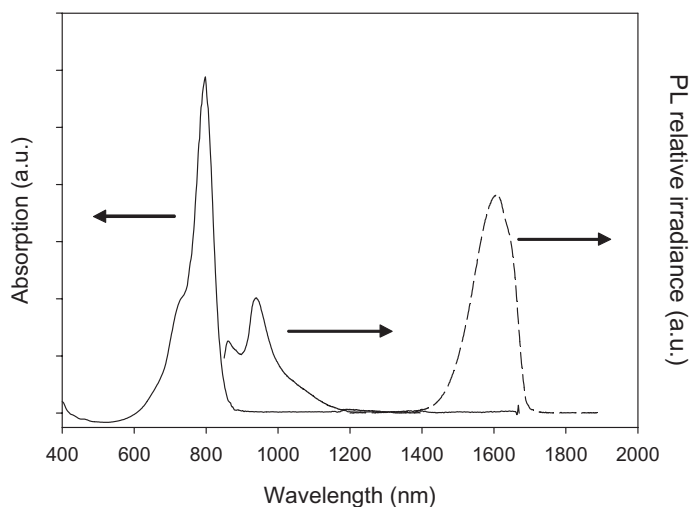


Figure 4. Spectra from a quantitative experiment to determine accurately the PL efficiency of one of our PbSe nanocrystal samples (a.u., arbitrary units). The absorption and PL spectra (—) of the cyanine dye, indocyanine green in DMSO, are shown together with the PL spectrum of the nanocrystals (---). In order to make a correct ‘photons-out–photons-in’ calculation of the PL efficiency, the variations in detector response and photon energy with wavelength must also be taken into account, as well as comparing the areas under the two PL spectra.

Table 1. Variation in the measured PL efficiency of aliquots taken from a typical synthesis of PbSe nanocrystals with growth time after injection.

Growth time (min)	PL efficiency (%)
3	61
5	36
7	27
9	23

where I_{sample} and I_{ref} are the irradiance spectra of the PL of the sample and reference dye, respectively, $R(\lambda)$ is the detector response function and ε is the nominal quantum yield of the reference dye. In our samples, we measured efficiencies as high as 60%, which compares favourably with other reported values [22, 23].

In table 1, we display values of PL efficiency as a function of growth time for a particular synthesis, as measured from aliquots of the reaction vessel. This shows a clear trend of the efficiency decreasing to the 20–30% level at longer growth times and we observe this behaviour to be typical within our record of syntheses. This effect may be due to extrinsic factors, such the residual presence of moisture or oxidizing agents in the reaction vessel during the dynamic phase of crystal growth, when a high fraction of surface sites in the nanocrystals may be uncoordinated at a given instant. Alternatively, variations in luminescence ‘blinking’ effects due to size-dependent Auger recombination effects, as commonly seen in quantum-dot systems [32], may also play a role.

4. Conclusions and future work

In this paper, we have described the successful implementation of a ‘one-pot’ organometallic precursor route to synthesizing colloidal PbSe nanocrystal quantum dots, in a way that has aided the understanding of several important issues relating to the dynamic phase of particle growth. Using a rigorously quantitative approach we find that solutions of these samples have PL quantum efficiencies as high as 60% in solution and that such highly efficient luminescence may be effectively optimized to coincide with the 1.3–1.55 μm telecommunications window by size tuning of the dots.

Work is currently in progress to investigate PL efficiencies in thin films of PbSe nanocrystals. It should be considered that, although high PL efficiencies in solution have been observed, such values are not likely from solid films of the nanocrystals. Indeed, in the case of reported measurements on matrix-free and matrix-bound films of CdSe nanocrystals, efficiencies of only about 1% are typical [33]. This is due to the much smaller distances between nanocrystals in such films relative to solution and, hence, the much higher probability of energy transfer of excitons between particles [34, 35] and the increased likelihood of sampling a non-radiative centre or ‘trap’ in the film. Instructive differences might be observable in the PbSe system, owing to the subtly different nature of the nanocrystal surface states and traps and also different Auger recombination rates.

In addition to the putative interest in using PbSe nanocrystals as an active gain medium in optical fibre amplifiers and photonic structures, we note a wide

range of different future applications and research directions. For example, the relatively unreactive nature of the uncoordinated surface states, as demonstrated by the high quantum yield and photostability, should facilitate the removal or refunctionalization of the capping layer to allow amphiphilic or even aqueous solubility, as has been demonstrated before for visible-light-emitting II–VI based nanocrystals [6, 36]. This may pave the way for the development of infrared-emitting biotags based on PbSe nanocrystals and, given the additional compatibility with silicon based microelectronics at these wavelengths, the development of integrated ‘biophotonics’ applications [37].

Acknowledgments

The authors would like to thank Jeffrey Peterson and Professor Todd D. Krauss of the University of Rochester, Rochester, New York, USA, for useful discussion and insight.

References

- [1] A.D. Yoffe, *Adv. Phys.* **42** 216 (1993).
- [2] A.P. Alivisatos, *J. Phys. Chem.* **100** 13 226 (1996).
- [3] A.P. Alivisatos, *Science* **271** 933 (1996).
- [4] A.L. Efros, M. Rosen, M. Kuno, *et al.*, *Phys. Rev. B* **54** 4843 (1996).
- [5] M. Grundmann, *Physica E* **5** 167 (2000).
- [6] M. Kuno, J.K. Lee, B.O. Dabbousi, *et al.*, *J. Chem. Phys.* **106** 9869 (1997).
- [7] T. Vossmeier, L. Kasikas, M. Giersig, *et al.*, *J. Phys. Chem.* **98** 7665 (1994).
- [8] A.A. Guzelian, U. Banin, A.V. Kadavanich, *et al.*, *Appl. Phys. Lett.* **69** 1432 (1996).
- [9] M. Achermann, M.A. Petruska, S. Kos, *et al.*, *Nature* **429** 642 (2004).
- [10] D.S. Ginger and N.C. Greenham, *Phys. Rev. B* **59** 10 622 (1999).
- [11] W.U. Huynh, J.J. Dittmer and A.P. Alivisatos, *Science* **295** 2425 (2002).
- [12] V.I. Klimov, A.A. Mikhailovsky, S. Xu, A. Malko, J.A. Hollingsworth, C.A. Leatherdale, H.J. Eisler and M.G. Bawendi, *Science* **290** 314 (2000).
- [13] C.E. Finlayson, D.M. Russell, C.M. Ramsdale, D.S. Ginger, C. Silva and N.C. Greenham, *Adv. Funct. Mater.* **12** 537 (2002).
- [14] M.V. Artemyev and U. Woggon, *Appl. Phys. Lett.* **76** 1353 (2000).
- [15] C.E. Finlayson, D.S. Ginger and N.C. Greenham, *Appl. Phys. Lett.* **77** 2500 (2000).
- [16] M. Bruchez, M. Moronne, P. Gin, *et al.*, *Science* **281** 2013 (1998).
- [17] U. Banin, Y.W. Cao, D. Katz and O. Millo, *Nature* **400** 542 (1999).
- [18] R.D. Schaller, M.A. Petruska and V.I. Klimov, *J. Phys. Chem. B* **107** 13 765 (2003).
- [19] E. Desurvire, *Erbium-Doped Fibre Amplifiers, Principles and Applications* (Wiley, New York, 2002).
- [20] C.B. Murray, D.J. Norris and A.P. Alivisatos, *J. Am. Chem. Soc.* **115** 8703 (1993).
- [21] X. Peng, M.C. Schlamp, A.V. Kadavanich and A.P. Alivisatos, *J. Am. Chem. Soc.* **119** 7019 (1997).
- [22] B.L. Wehrenberg, C. Wang and P. Guyot-Sionnest, *J. Phys. Chem. B* **106** 10 634 (2002).
- [23] H. Du, C. Chen, R. Krishnan, *et al.*, *Nano Lett.* **2** 1321 (2002).
- [24] U.K. Gautam and R. Seshadri, *Mater. Res. Soc. Bull.* **39** 669 (2004).
- [25] C.B. Murray, S.H. Sun, W. Gaschler, *et al.*, *IBM J. Res. Dev.* **45** 47 (2001).
- [26] A. Sashhiuk, L. Langof, R. Chaim and E. Lifshitz, *J. Cryst. Growth* **240** 431 (2002).
- [27] P.W. Voorhees, *A. Rev. Mater. Sci.* **22** 197 (1992).
- [28] I. King and F.W. Wise, *J. Opt. Soc. Am. B* **14** 1632 (1997).
- [29] L. Banyai and S.W. Koch, *Semiconductor Quantum Dots* (World Scientific, Singapore, 1993).

- [30] A.D. Andreev, E.V. Kolobkova and A.A. Lipovskii, *J. Appl. Phys.* **88** 750 (2000).
- [31] N.C. Greenham, I.D.W. Samuel, G.R. Hayes, *et al.*, *Chem. Phys. Lett.* **241** 89 (1995).
- [32] M. Kuno, D.P. Fromm, H.F. Hamann, *et al.*, *J. Chem. Phys.* **112** 3117 (2000).
- [33] C.E. Finlayson, *Optical characterization of semiconductor nanocrystals*, PhD thesis, Cavendish Laboratory, University of Cambridge, UK (2001).
- [34] T. Förster, *Ann. Phys. Leipzig VI* **2** 55 (1948).
- [35] C. Kagan, C.B. Murray and M.G. Bawendi, *Phys. Rev. B* **54** 8633 (1996).
- [36] W.C.W. Chan and S. Nie, *Science* **281** 2016 (1998).
- [37] P.N. Prasad, *Introduction to Biophotonics* (Wiley-Interscience, New York, 2003).